ADAPTIVE MESH GENERATION FOR AXISYMMETRIC MAGNETOSTATIC SOLUTIONS

Kartik Sitapati
Senior Member, IEEE

Abstract—An error estimation technique based on the L2 error norm is implemented in this paper for axisymmetrical magnetostatic finite-element analysis using the magnetic potential. The adaptive mesh generated by this error estimator is tested on three commonly used FEA formulations and the results are compared. Convergence of both the global and local errors are used as indicators. The air gap where force is to be computed is refined based on the rate of change in the calculated force rather than the flux density. Results that highlight the accuracy of the combined methods for force calculations are displayed for a solenoid actuated valve with non-linear FEA.

Index Terms—FEA, error, L2 norm, adaptive mesh, axisymmetric, air gap, force, flux density, magnetic potential.

I. Introduction

Modern finite-element analysis (FEA) includes a posteriori error estimation techniques to provide an indication of the relative error, and to refine the mesh so as to improve the accuracy. Error estimation methods used in mechanics are usually applied in magnetostatics with some modifications. The modifications include variations of the Zienkiewicz-Zhu (Z-Z) method. The main drawback of the Z-Z method is inadequate refinement in domains consisting of multiple materials. An alternative error estimation technique used in mechanics based on the L2 norm is implemented in this paper and works well with multiple materials. The local error is used for mesh refinement. Its effectiveness in magnetostatics is displayed using a solenoid design as an example. Even small error magnitudes in the flux density in air gaps usually results in large inaccuracies in the calculated forces. The air gap is refined by the rate of change in the force.

II. Axisymmetric FEA

Axisymmetric magnetostatic solutions can be obtained by using the scalar magnetic potential. Three different developments are shown below with equations describing each coefficient of the stiffness matrix and source vector.

$$\prod(\bar{A}) = -\int_{\Omega}\frac{1}{\mu}\left[\left(\frac{\partial A_{\phi}}{\partial z}\right)^2+\frac{1}{r^2}\left(\frac{\partial(rA_{\phi})}{\partial r}\right)^2\right]d\Omega+2\int_{\Omega}A_{\phi}J_{\phi}d\Omega \quad (1)$$

The functional without Neuman boundary conditions is in cylindrical coordinates, (r, φ, z). Aφ and Jφ are the magnetic potential and the source current respectively. μ is the permeability of the material. Note that dΩ = 2πrdrdz. Oncea solution for Aφ has been obtained, the flux density in each element is found using

$$\bar{B}^e = \nabla\times\hat{\phi}A_{\phi} = -\hat{r}\frac{\partial A_{\phi}}{\partial z}+\hat{z}\frac{1}{r}\frac{\partial\left(rA_{\phi}\right)}{\partial r} \quad (2)$$

Aφ is expanded as Aφ = XM i NiAi where Ni are the scalar bases and testing functions. M is the number of nodes in the mesh. A. Direct Solution The direct solution results from the first variation of (1) which is

$$\int_{\Omega}\frac{1}{\mu}\left[\left(\sum\frac{\partial N_i}{\partial z}A_i\right)\frac{\partial N_j}{\partial z}+\frac{1}{r^2}\left(\sum\left(r\frac{\partial N_i}{\partial r}+N_i\right)A_i\right)\left(r\frac{\partial N_j}{\partial r}+N_j\right)\right]d\Omega - \int_{\Omega}N_jJ_{\phi}d\Omega = 0 \quad (3)$$

The equation for the terms in the stiffness matrix and source vector is

$$\int_{\Omega^e}\left[r\frac{\partial N_i}{\partial z}\frac{\partial N_j}{\partial z}+r\frac{\partial N_i}{\partial r}\frac{\partial N_j}{\partial r}+N_i\frac{\partial N_j}{\partial r}+\frac{\partial N_i}{\partial r}N_j+\frac{1}{r}N_iN_j\right] \frac{1}{\mu}A_i drdz-\int_{\Omega^e}rN_jJ_{\phi}drdz = 0 \quad (4)$$

The subscripts, i and j, span the entire mesh. Ωe implies that the integral is over an element of the mesh.

B. Similar to 2-D Magnetostatics In this formulation, the equation for 2-D magnetostatics is directly used after replacing the coordinate variables, x = r and y = z. The functional for 2-D magnetostatics in cartesian co-ordinates without Neuman boundary conditions is

$$\prod(\bar{A}) = -\int_{\Omega}\frac{1}{\mu}\nabla\times\bar{A}_z\cdot\nabla\times\bar{A}_z d\Omega + 2\int_{\Omega}\bar{A}_z\cdot\bar{J}_z d\Omega \quad (5)$$

A new potential is defined as

$$U = rA \Rightarrow A = \frac{U}{r} \quad (6)$$

After the taking the first variation, the equation for the terms in the stiffness matrix and source vector is

$$\int_{\Omega^e}\left[\frac{\partial N_i}{\partial y}\frac{\partial N_j}{\partial y}+\frac{\partial N_i}{\partial x}\frac{\partial N_j}{\partial x}\right]\frac{1}{\mu'}U_i d\Omega^{e'} - \int_{\Omega^e} N_j J_\phi d\Omega^{e'} = 0 \quad (7)$$

where $\mu' = \mu r$ and $dxdy = d\Omega^{e'}$.

C. Change of Variables A change of variables is made to both the potential and source to eliminate any terms containing r in the denominator

$$A = \sqrt{r}U \Rightarrow U = \frac{A}{\sqrt{r}} \qquad J_\phi = \sqrt{r}\mathcal{J} \Rightarrow \mathcal{J} = \frac{J_\phi}{\sqrt{r}} \quad (8)$$

The first variation results in

$$\int_{\Omega^e}\left[r^2\left(\frac{\partial N_i}{\partial z}\frac{\partial N_j}{\partial z}+\frac{\partial N_i}{\partial r}\frac{\partial N_j}{\partial r}\right)+\frac{3r}{2}\left(N_i\frac{\partial N_j}{\partial r}+\frac{\partial N_i}{\partial r}N_j\right)+\frac{9}{4}N_iN_j\right]\frac{1}{\mu}U_i drdz - \int_{\Omega^e} r^2 N_j\mathcal{J} drdz = 0 \quad (9)$$

for the stiffness and source vector matrices. The potential is recovered after the matrix solution when a transformation has been used as in (7) and (9).

III. L2 Norm Error Calculation

The smoothed or averaged flux density value at each node is first calculated from the FEA results. Separate nodal values are computed for nodes on boundaries between different material properties. The smoothed norm is defined as

$$W_s = \sqrt{\frac{\sum_{n=1}^{N_e}\left(\int_{\Omega^e}\bar{B}^e_{sn}\cdot\bar{B}^e_{sn}d\Omega^e\right)}{N_e}} \quad (10)$$

where N_e is the number of elements in the mesh, $\bar{B}^e_{sn}$ is the smoothed flux density interpolated at the center of element n. The local error in element n is computed using

$$e_n = \frac{\sqrt{\int_{\Omega^e}(\bar{B}^e_{sn}-\bar{B}^e_n)\cdot(\bar{B}^e_{sn}-\bar{B}^e_n)\,d\Omega^e}}{W_s}100\% \quad (11)$$

where $\bar{B}^e$ is the flux density obtained directly from the FEA results and is piece-wise constant with first order triangles. Note that the permeability is not used in the calculations. The local error is used to refine the mesh until it is lower than a user specified tolerance. By not using the permeability in the calculated errors, refinement in multiple materials is easily obtained based only on the rate of change of the flux density

IV. Air Gap Force Error Calculation

The rate of change of the flux density in the air gap where force values are to be estimated may not be high enough to obtain adequate refinement based on the norm error described in the previous section. A thin layer is created in the air gap and a secondary error computing mechanism is used. The force in the air gap is a function of the radial and ˆz components of the smoothed flux density, i.e., F = f (Br , Bz). The force is calculated in each element at all three corner nodes when firstorder triangles are used. The maximum value of all elements in the layer is stored as F e max . The nodal force error between nodes in each element is calculated

$$F^e_{err} = \frac{F^e_i - F^e_j}{F^e_{max}}100\% \quad (12)$$

where i and j span the three nodes of each element. If any of the three errors is greater than a user specified value, the element is marked for refinement. This process continues until there are no errors that are greater than the specified value. V. Mesh Refinement The mesh is refined using the error norm and provides good refinement in areas where the flux density changes rapidly. The air gap region where force is to be computed is refined based on the force errors. The Delaunay triangulation property and user defined triangle quality constraints are respected in each mesh via element quality checks during refinement. A robust mesh generator capable of fine refinement is mandatory to ensure accurate results. The procedure is summarized as 1) Generate initial mesh 2) Perform finite element analysis, post process and compute errors 3) Mark elements that require refinement and split triangles 4) Ensure Delaunay criteria and mesh quality are maintained, if not perform maintenance 5) Provide refined mesh back to the FEA engine Steps 2-5 are repeated, exit is at step 2. VI. Test Solenoid Actuator The main dimensions of the solenoid which works with bidirectional direct current were already determined by the application. When energized, the solenoid actuates a normally open valve via the stem and closes it. A spring forces the plunger

back to the normally open position upon de-energization. The entire plunger cavity is filled with hydraulic fluid and this solenoid-valve is designed for use in the hydraulic system in an airborne application. The cross section of the axisymmetric model is shown in Fig. 1. All magnetic parts were made from

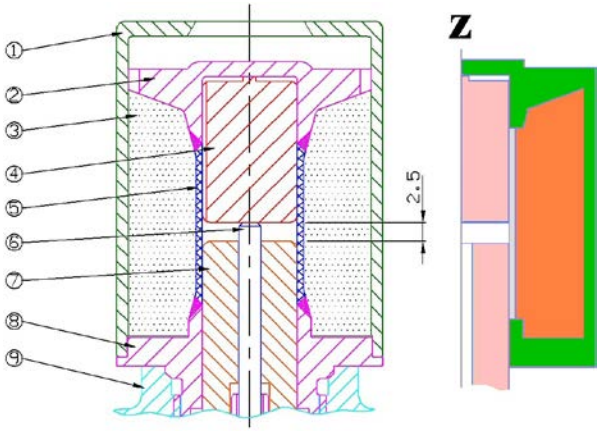

Fig. 1. Cross section of the solenoid (left) and FEA model (right). Electrical insulation material has not been shown. 1) Magnetic housing, 2) Magnetic top end plate, 3) Coil, 4) Magnetic plunger, 5) Non-magnetic spacer tube, 6) Valve stem (non-magnetic), 7) Stationary magnetic insert, 8) Magnetic bottom end plate, 9) Valve body. The air gap height is 2.5 mm. All sharp edges were eliminated in the production version. the same carbon steel material and the coil is wound with 2150 turns. Fig. 2 shows the layers used for force calculation

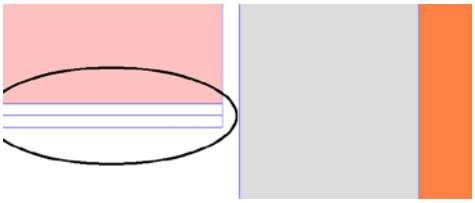

Fig. 2. Detail of the air gap showing two layers. The force is calculated in the lower layer. The height of the layers can be varied and the layers are formed below the plunger. The force calculation can be done on the entire plunger as well but requires unacceptable convergence time.

VII. Results The tolerances for the error in flux density and the air gap force were set at 12 and 3 % respectively for adaptive FEA. The minimum element area during refinement was restricted to 1 −18 sq. m. Each solution at a particular plunger position converged after 15 to 25 steps. Fig. 3 shows a typical convergence plot of the air gap force error. For a given error tolerance, convergence can be achieved at much faster rates in linear magnetostatics. The rate of convergence is a function of the saturation level of magnetic steel and the strength of enforcement of refinement which was maintained at a weak level. The overall rate of convergence was best with method (B), then method (A), and followed by method (C) which was slower by a factor of 4. This section displays the results

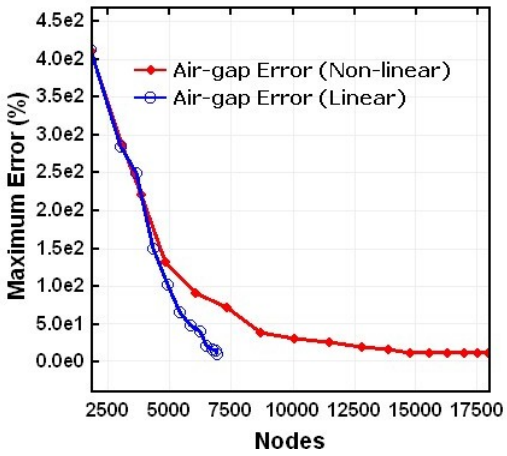

Fig. 3. Convergense of the air gap force error with adaptive steps using method (C). The nonlinear case has 18 steps while the linear case has 12 steps. obtained with the methods described earlier. A. Adaptive Mesh Fig. 4 shows the adaptive mesh generation based on FEA error. The mesh is based on method (C) and the air gap mesh refinement is not shown for brevity. It can clearly be seen that the mesh is only refined in areas that require refinement and it can also be observed that the Delaunay condition provides refinement in areas not marked such as in the coil. This helps to reduce the local error with global changes and improves the overall quality of the results

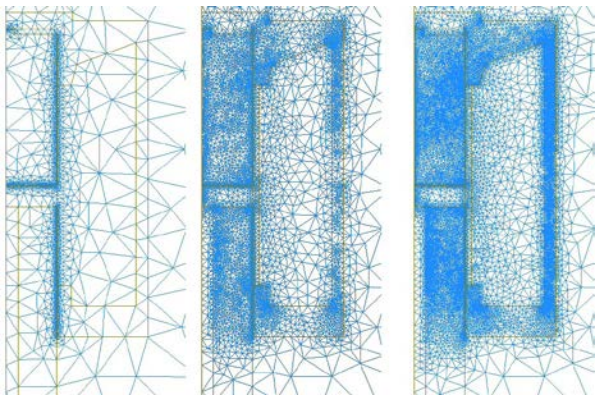

Fig. 4. Initial mesh with ∼2500 nodes (left), intermediate mesh after 5 steps (center), final mesh with ∼20000 nodes after 18 steps (right). B. Fields The Flux contours are shown in Fig. 5 and are nearly identical. Unlike 2-D magnetos-

tatics in cartesian coordinates, the contour plots in the axisymmetric case cannot be relied on to provide an accurate indication of the actual flux paths due to the factor r in (2). The results for all three methods are similar. Each method has a different number of unknowns as the adaptive mesh generation produces different errors. While the results for the flux density appear to be the same, the total convergence time is very different.

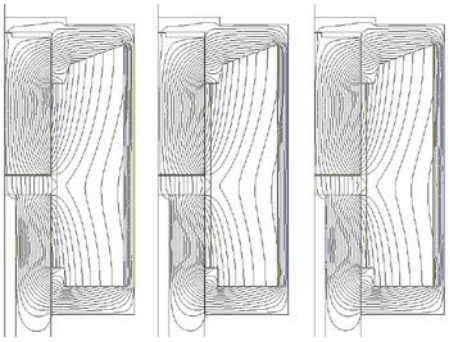

Fig. 5. Magnetic potential contour plots with identical limits for all three methods. Method (A) (left), method (B) (center), method (C) (right). The limits span the entire range from zero to the maximum value of the potential with equal intervals. Figs. 6 and 7 show the flux density vector and the flux density. The flux density is the smoothed value obtained by gradient recovery and is piecewise-linear. The magnetic circuit is not saturated and is within the flux carrying capability of the materials chosen. The arrow plot shows that there is no significant leakage other than in the air gap region. Fig. 8 shows the flux density calculated at a small distance above the air gap with the plunger at its default position. C. Force The force in the air gap with varying air gap height is show in Fig. 9. A constant current is fed into the coil. Thedirect axisymmetric solution and the method based on the 2- D magnetostatic solution provide nearly identical results at all positions.

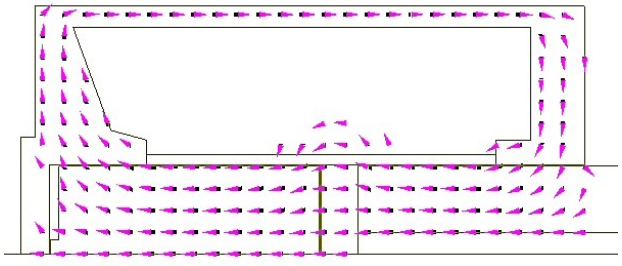

Fig. 6. Plot showing the flux density vectors. The solenoid has been rotated by 90o in the CCW direction. The air gap is at its maximum height of 2.5 mm.

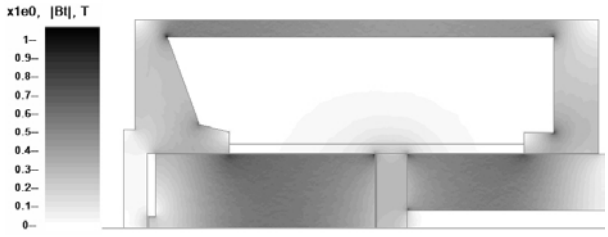

Fig. 7. Plot showing the magnitude of flux density. The solenoid has been rotated by 90o in the CCW direction. Exact interpolation has been used to plot the piecewise-linear recovered flux density with 24 shades of grey.

VIII. Conclusion

An error estimation technique that combines both the flux density error and force error for mesh refinement in axisymmetric finite-element analysis was described with a solenoid as an example. It was shown that efficient mesh refinement is obtained so that the overall error is reduced while keeping the number of unknowns to a minimum. Accurate force calculations are obtained as the force error itself is used for mesh refinement in regions where force is to be computed. The method based on the 2-D magnetostatic solution proved to be the most efficient of the three axisymmetric solutions that were tested. This paper is an extension to axisymmetric problems of the techniques described in [7]. The torque error is replaced by the force error here.

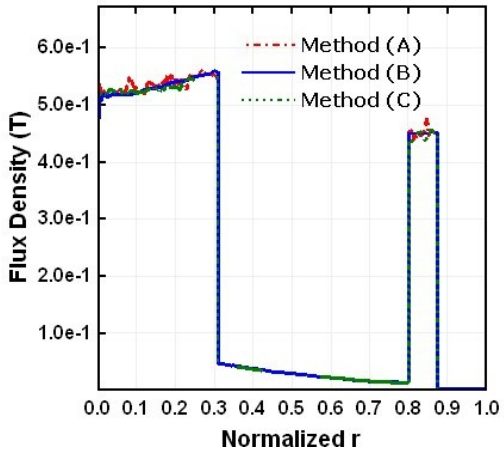

Fig. 8. Flux density plot with all three methods at a constant z and normalized r. The constant z value is chosen such that it passes through the plunger. While all three methods provide similar results, method (B) which is based on the symmetric 2-D magnetostatics solution provides the smoothest curve. The flux density increases in the plunger with increasing radius, then be-

comes close to zero in the coil, then increases again in the return path of the housing, and then drops to zero outside the solenoid body.

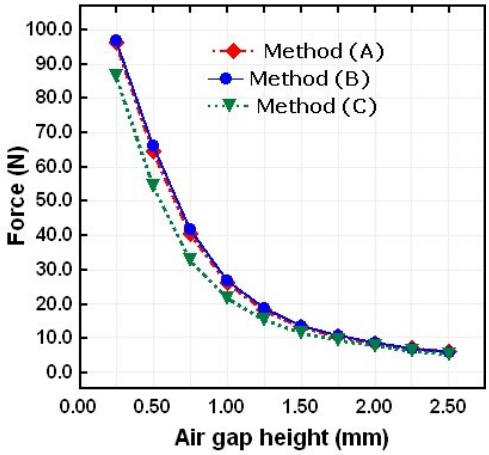

Fig. 9. Force calculated by all three methods using non-linear FEA with varying air gap height. Methods (A) and (B) provide similar results at all positions, method (C) provides lower values. The measured values agree closely with methods (A) and (B) but are not shown.

References

[1] Mark Ainsworth and Tinsley J. Oden. A Posteriori Error Estimation in Finite Element Anaysis. John Wiley & Sons, New York, NY, 2000.

[2] Nicola Bianchi. Electrical Machine Analysis using Finite Elements. CRC Taylor & Francis, Boca Raton, FL, 2005.

[3] Robert D. Cook, David S. Malkus, Michael E. Plesha, and Robert J. Witt. Concepts and Applications of Finite Element Analysis. John Wiley & Sons (Asia), Singapore, fourth edition, 2003.

[4] B. Forghani, D. A. Lowther, P. P. Silvester, and G. O. Stone. Newtonraphson finite element programs for axisymmetric vector fields. IEEE Trans. Magn., Vol. 19(6):pp. 2523–2526, Nov. 1983.

[5] Shinya Matsutomo, Tomoyuki Miyamoto, Kazufumi Kaneda, So Noguchi, and Hideo Yamashita. An error evaluation scheme based on rotation of magnetic field in adaptive finite element analysis. IEEE Trans. Magn, Vol. 42(4):pp. 567–570, Apl. 2006.

[6] Robert D. Pillsbury Jr. NMLMAP- a two dimensional finite element program for transient or static, linear or nonlinear magnetic field problems. IEEE Trans. Magn, Vol. 18(2):pp. 406–410, Mar. 1982.

[7] Kartik Sitapati. Air-gap layers and adaptive mesh generation for torque calculations in rotating electrical machines. Presented at ICEM 2008, Vilamoura, Portugal, September 2008.

[8] Song-Min Wang, Takashi Miyano, and Mont Hubbard. Electromagnetic field analysis and dynamic simulation of a two-valve solenoid actuator. IEEE Trans. Magn., Vol. 29(2):pp. 1741–1746, Mar. 1993.